











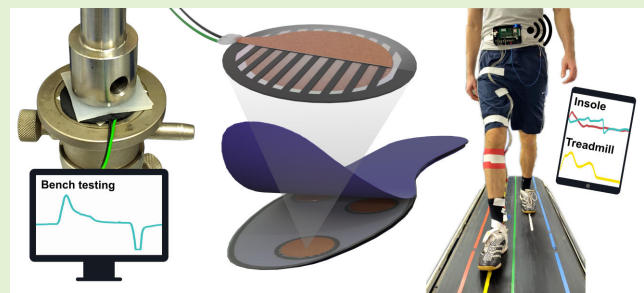


# 3D-Printed Piezoelectric PLA-Based Insole for Event Detection in Gait Analysis

Bastian Latsch , Niklas Schäfer , Martin Grimmer , Omar Ben Dali , Omid Mohseni ,  
 Niklas Bleichner , Alexander A. Altmann , Stephan Schaumann , Sebastian I. Wolf ,  
 André Seyfarth , Philipp Beckerle , *Senior Member, IEEE*, and Mario Kupnik , *Senior Member, IEEE*

**Abstract**—Detecting human movement is crucial for the control of lower limb wearable robotics designed to assist daily activities or rehabilitation tasks. Sensorized insoles present a viable option for extracting control inputs, such as gait events and the corresponding phases, essential for regulating the magnitude and timing of assistance. Given their highly sensitive piezoelectric response to dynamic loading, ferroelectrets emerge as a cost-effective solution for customizing sensors suitable for these autonomous systems. Within this study, an insole with four ferroelectret sensors is 3D-printed monolithically from polylactic acid (PLA) onto bulk films of the same material through seamless thermal fusion. Sensor and insole are characterized through a testing machine and by conducting human walking experiments on an instrumented treadmill. The testing machine results indicate suitable sensor performance for the application in wearable robotics concerning the sensitivity, minimal detectable change, hysteresis, drift, and repeatability. Walking experiments reveal the insole's capability to detect gait events such as heel strikes with minimal variability and on average 16 ms faster compared to the reference of vertical ground reaction forces across all walking speeds above 1 m/s. The peak sensor outputs strongly relate to the reference while both exhibit a linear ( $R^2 > 95\%$ ) increase corresponding to walking speed. In conclusion, study findings demonstrate the feasibility of PLA-based ferroelectrets as customized insole sensors for event detection in gait analysis, enabling assessment of human biomechanics with minimal impact on the natural gait and control of autonomous wearable robotics, such as exoskeletons.



**Index Terms**—Gait analysis, legged locomotion, gait event detection, 3D-printed piezoelectric sensor, ferroelectret insole

## I. INTRODUCTION

**G**AIT phase detection during human gait holds a pivotal position across a spectrum of scientific domains, encompassing biomechanics and gait analysis, robotics and control, rehabilitation and assistive devices, as well as sports

performance evaluation [1]–[4]. Humans utilize cutaneous receptors located in the foot sole [5] and proprioceptors in the muscles [6] to perceive tactile and contact information with the environment to control their movements [1]. In technical settings, sensors are employed to capture this valuable data concerning the human gait.

The gait phase, the progress within a stride, serves as a key information source in analyzing the variety of human movement tasks, aids in identifying gait characteristics, and offers effective control of gait patterns in robotic locomotion [7]. In particular, gait phase detection is crucial for real-time control of exoskeletons, synchronizing their motion to the wearer's movements [8]. Other research shows that exoskeletons, which are capable of responding even faster than the user's physiological reaction, improve disturbance compensation in balance [9], emphasizing the relevance of fast event detection. Given the importance of gait phase detection, the capability to identify gait phases in a user-friendly and portable manner holds immense potential.

Through its direct link to acceleration, the ground reaction force (GRF) offers quick information about impending changes in motion, which is crucial for providing real-time feedback control for legged robots [10]. GRF serves as an

Manuscript received 15 May 2024; accepted 17 June 2024. This work was supported in part by the Deutsche Forschungsgemeinschaft (DFG) under grant no. 509096131 and no. 450821862. The authors thank Felix Herbst for his help with the image creation, the students Youssef Sellami, Steffen Graffe, and Esan Sundaralingam for their support with the insole and measurement preparation.

B. Latsch, N. Schäfer, O. Ben Dali, O. Mohseni, A. A. Altmann, S. Schaumann, and M. Kupnik are with the Measurement and Sensor Technology Group, Technische Universität Darmstadt, 64283 Darmstadt, Germany (e-mail: [mario.kupnik@tu-darmstadt.de](mailto:mario.kupnik@tu-darmstadt.de)).

M. Grimmer is with the Cyber-Physical Systems Laboratory, Technische Universität Darmstadt, 64283 Darmstadt, Germany.

M. Grimmer, O. Mohseni, and A. Seyfarth are with the Locomotion Laboratory, Institute of Sports Science, Technische Universität Darmstadt, 64289 Darmstadt, Germany.

N. Bleichner and S. I. Wolf are with the Department for Motion Analysis, Clinic for Orthopedics and Trauma Surgery, Heidelberg University Hospital, 69118 Heidelberg, Germany.

P. Beckerle is with the Chair of Autonomous Systems and Mechatronics, Friedrich-Alexander-Universität Erlangen-Nürnberg, 91052 Erlangen, Germany.

Copyright 2024 IEEE. Publisher-DOI: 10.1109/jsen.2024.3416847.

objective, quantifiable measure for optimizing the control of wearable robotic devices [11]. This capacity has driven the development of GRF-based controllers for various joints in robots, exoskeletons, and prostheses, resulting in the generation of stable gaits and in enhanced human locomotion assistance [12]–[14].

The terminology of gait phases used throughout this work is based on the definitions provided by Perry and Burnfield [15]. During the stance phase, the foot is in contact with the ground; mid-stance describes when it is flat on the ground. The swing phase is the part when the foot is not on the ground. One stride represents the entire cycle of a walking motion, starting with the heel strike event when one foot initially contacts the ground and ending when the same foot touches the ground again. One stride of human walking at an average speed of  $1.3 \text{ m s}^{-1}$  lasts about 1.1 s [16]. At around 60% of the stride, the toe-off event takes place as the terminal contact during lift-off of the foot [15]. Even if the anterior-posterior and medial-lateral forces on the foot sole are important for a stable gait, the main component of the appearing forces is the vertical GRF. It results from the gravitational acceleration and shows dynamic peaks during walking of around 120% of the still-standing body weight [16]. Detecting the heel strike and toe-off events can be achieved by applying a force threshold on the vertical GRF obtained from sensors, such as in force platforms and insoles [17].

While wearable gait event detection is possible with inertial measurement units (IMUs) as well [2], [18], [19], insoles offer the acquisition of spatial pressure distribution under the foot sole [20]. Among the most used insoles in clinical studies are the commercially available systems F-Scan [21], Pedar [22], Loadsol [23], and Moticon [24]. These are often taken as a reference for the validation of custom-built insole systems in research if force measurement plates are not feasible in case of mobile experimental setups.

By monitoring foot pressure and walking patterns, medical issues can be pointed out even before any inconvenience is induced, thus, supporting the prevention of disease conditions [25]. For instance, real-time feedback can be provided to address concerns such as overpronation or supination, potentially averting related foot and ankle complications [26]. Furthermore, multi-axial measurements in insoles, including shear forces, are of interest to achieve the same capabilities of force measurement plates with mobile solutions. Wang et al. build 64 inductive sensor elements into their insole to measure shear forces in addition to the normal component [20]. The system is perceived to be comfortable by the participants and plantar normal pressure is measured with an RMS error of 2.1%. The tedious sensor calibration due to the large number of sensors is described as an inconvenience of the current system and differences in the insole interface, such as socks and shoes, cause discrepancies between participants.

The placement and size of the sensors in the insole is determined by the application needs, with most comprising a heel sensor. The number of insole sensors ranges from two [27] up to 64 [20]. While a high spatial resolution may be beneficial in certain scenarios, a relative pressure measurement is possible with only three sensors at the forefoot, midfoot, and

hindfoot [28], [29]. Even though the same sensor technologies are used for plantar pressure measurements as decades ago [30], creating affordable and resilient sensorized wearable systems that effectively capture interaction forces continues to pose a significant challenge [31].

Plantar pressure measurement principles can be classified into piezoresistive [27], [32]–[35], capacitive [22]–[24], inductive [20], [36], piezoelectric [37]–[40], optical [41], [42], and other less frequently used emerging sensor technologies [43].

Most of the insoles in the literature use piezoresistive principles due to their easy availability or capacitive sensors for their high accuracy. Piezoresistive insoles are often based on force-sensing resistors (FSRs) [27], [32], which in general facilitate simple electronic read-out circuits. Other methods include pressure-sensitive rubbers [44] and polymeric films impregnated with carbon black, known as Velostat or Linqstat, [45], [46]. Regardless of improvements in the read-out and the design of piezoresistive sensors [21], [47], [48], the general quality compared to other sensor technologies regarding creep, accuracy, and repeatability is low [49]–[51]. In a study that utilizes FSR sensors to trigger functional electrical stimulation in children with cerebral palsy, 5.5% of the steps are not detected at all, with 80% of these missed due to a smaller than expected signal below the detection threshold programmed [32]. Shu et al. estimate the participant's body weight utilizing a piezoresistive strain sensing fabric with an average deviation of 6.9%, while the sensor's accuracy and zero drift are specified with 5%, respectively [34]. Lin et al. employ a piezoresistive textile, made from yarn coated with a piezoelectric polymer, to build a matrix insole with 48 sensors covering 80% of the foot sole area [35]. They calculate the numerical derivative of the sensor voltage to detect heel strike and toe-off events independently from the sensor offset and participant weight.

Because of its dynamic nature, the piezoelectric effect is frequently utilized in gait analysis, either through hard ceramic sensors from materials such as lead zirconate titanate (PZT) or flexible polymer sensors. Piezoelectric polymer sensors, typically made from polyvinylidene fluoride (PVDF), are superior to ceramic-based sensors for the application in wearables due to their flexibility, adaptability to the human foot, and non-toxic properties [52]. Rajala et al. utilize PVDF sensors with a charge amplifier to obtain the pressure from eight locations under the foot [40]. Deng et al. present a piezoelectric insole based on PVDF pressure sensors with a sensitivity of  $23 \text{ pC N}^{-1}$  and describe it as a self-powered system [37]. They use a 2 kg metal cylinder to simulate a foot roll but no human experiment is conducted. Simultaneous charging, measuring, and data transmission seems not to be tested.

Recently, polymers with low inherent piezoelectricity, such as polypropylene (PP) and polylactic acid (PLA), are used to 3D print structures with well-defined air cavities [53], [54]. After the activation with charging techniques such as corona or contact charging, the cavities form the sensor based on the piezoelectric effect, also referred to as ferroelectret [52]. During deformation, the embedded compressible air cavities enhance the charge displacement within the cellular material yielding a higher quasi-piezoelectric effect with a comparable

charge stability sufficing for long-term use and piezoelectric coefficients of up to  $22\,000\text{ pC N}^{-1}$  [52], [55]–[57]. The sensitivity of PLA-based ferroelectrets is exceptional compared to that of sensors made from inorganic piezoelectric materials, such as PVDF [52], [58]. In addition, PLA is known as a bio-compatible and biodegradable polymer [58]–[62]. Furthermore, using PLA for the sensor offers great customizability through 3D printing and a higher sensitivity than other flexible materials.

In this work, we introduce a PLA-based ferroelectret sensor to detect gait events by placing it in a sensorized insole under the foot. Due to their piezoelectric nature, the sensor elements can operate without any power supply, thus reducing the number of wires. The focus of this work is the characterization and a proof-of-concept application for this sensor, not a user study. Compared to our previous conference proceedings publication [63], we utilize eco-friendly PLA that can be synthesized from renewable resources [59] instead of PP. Concerning the sensor design, the sensor elements are completely redesigned to withstand the body weight and characterized with significantly larger forces of over 800 N, compared to 10 N in earlier versions [64].

We assess the sensor properties focusing on sensitivity, measurement range, hysteresis, repeatability, zero drift, and full-scale drift and deduce the sensor's electromechanical behavior with its output in relation to the applied force, expecting a characteristic that is well-suited for dynamic force measurements. Subsequently, we validate the applicability of the sensor for gait event detection in an experiment by integrating four sensors into an insole, which is worn by one human participant walking on an instrumented treadmill. The sensor data is evaluated for the possibility to determine the gait events heel strike and toe-off by using the vertical GRF of the treadmill as a reference. We choose not to use motion capture systems as a reference for comparing our insole's detection. Several studies already compared ground reaction forces with motion capture during human gait [65], [66], and multi-axial force measurement platforms, as incorporated into the treadmill, are considered the gold standard for measuring pressure under the foot. We anticipate good detection of the heel strike, as it causes an abrupt change in the signal, while the detection of the toe-off event may be less clear due to the gradual relief of weight. Altogether, the characterization of our autonomous insole system will lay the foundation for its application in gait analysis and wearable robotics control.

## II. FERROELECTRET INSOLE SENSOR

We first delineate the sensor design and preparation, followed by the description and the test of the acquisition circuit. Next, we thoroughly examine the sensor output in static and dynamic test conditions to comprehensively assess its performance for the intended application. In the insole application, the absolute sensor outputs will vary from one person to another as the viscoelastic properties of the foot sole differ [67] and the sensor itself can depend on the interfacing material as well [64]. However, in gait analysis, absolute measurements of GRFs may be less relevant compared to distinct

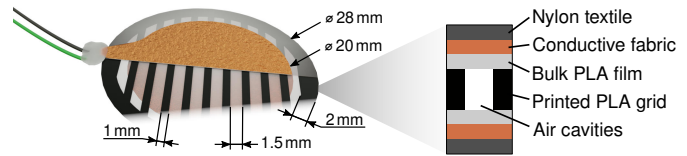


Fig. 1. The sensor consists of two bulk PLA films and a structured 3D-printed PLA layer, which contains the air cavities for charge trapping.

signal attributes that hold greater significance for identifying patterns and associated ailments [11]. Therefore, the relative signal distribution is of greater significance here, which we investigate in the sensor characterization. Subsequently, we demonstrate the sensor's applicability as a proof-of-concept in an insole walking scenario with ground truth data obtained from an instrumented treadmill.

### A. Sensor Design and Preparation

The sensor structure (Fig. 1) is designed using Fusion 360 (Autodesk, San Rafael, CA, USA). We employ PrusaSlicer (Prusa Research, Prague, Czech Republic) to prepare the 3D printing process and produce the structure with a commercially available printer for fused filament fabrication (i3 MK3S, Prusa Research, Prague, Czech Republic).

The process begins by affixing a bulk PLA film (Maropack, Andernach, Germany), 0.02 mm thick, onto the print bed, which is heated up to  $60^{\circ}\text{C}$  to thermally strain the film [64]. We use bulk films and filament of the same material to attain a seamless thermal fusion during the print process [64]. A circular PLA structure with a 2-mm-wide outline and 28 mm outer diameter [64] is printed onto the heated film using standard settings for the black PLA filament (Redline Filament, Neuss, Germany). This structure includes a grid of parallel ridges, each 1 mm wide and 1.5 mm apart. It consists of a single 0.2-mm-thick layer, printed with a nozzle diameter of 0.4 mm and a print speed of  $20\text{ mm s}^{-1}$ . The temperature of the extruded PLA surpasses the melting point of the film, causing the materials to fuse upon contact. The bulk film's thermal strain is preserved due to the print bed's heat, pre-stressing the film. Next, another PLA film on a second pre-heated print bed ( $100^{\circ}\text{C}$ ) is thermally bonded ( $100^{\circ}\text{C}$  for 30 s) on top of the printed structure using a manual heat press (1250 W, Vevor, Paris, France). The printed grid pattern forms the well-defined air cavities, preserves the distance between the films as a spacer, and maintains the thermal straining effect after cooling [55].

We cut electrodes of 20 mm diameter from a self-adhesive conductive fabric and solder wires to it. The solder point is placed on the rigid outer part of the sensor, distant from the cavities, i.e., the actual sensor surface. This prevents the solder point from interfering with the measurement. The electrodes are placed on both sides of the sandwich structure. A high voltage source (HCN 14-12 500, FuG Elektronik, Germany) applies 4 kV across them for contact charging, initiating Paschen breakdown in the air voids and creating dipoles at the PLA to air interfaces, which turns the structure into a ferroelectret [68]. After short-circuiting the electrodes, the sensor is neutrally charged to the outside and generates

outputs through deformation in the extra-low voltage range, which is harmless to humans. In the last step, we use self-adhesive nylon textile as cover material on both sides to encase the ferroelectret and protect it from environmental influences.

## B. Data Acquisition

The deformation of the sensor structure by a force causes a displacement of the trapped charges inside the air cavities resulting in induced mirror charges on the electrodes. The sensor output reflects this charge displacement within the ferroelectret. This behavior is defined as a pseudo-piezoelectric effect [69]. Therefore, the relation between force  $F$  on the sensor and its charge output  $Q$  can be defined using

$$Q = d_{33} \cdot F, \quad (1)$$

with the longitudinal piezoelectric coefficient  $d_{33}$  that relates between the mechanical and electrical domain in the main force direction. We measure the voltage that results from the charge generated when the sensor is stressed as

$$\frac{dQ}{dt} = I = \frac{V}{Z}, \quad (2)$$

where  $I$  is the current induced during time  $t$ , and  $V$  is the voltage drop across the equivalent input impedance  $Z$  of the measurement device. Combining (1) and (2) results into

$$V(t) = Z \cdot d_{33} \cdot \frac{dF}{dt}. \quad (3)$$

Hence, an analytical computation is achievable through modeling the electrical circuit ( $Z$ ) and the piezoelectric sensor behavior ( $d_{33}$ ). The detailed analytical computation is beyond the scope of this paper. Solely the direct proportionality between the force derivative and the sensor output  $V$  is of significant relevance for the intended application.

Typically, electrometers or charge amplifiers are utilized to detect and measure small charges with high accuracy. Electrometers with their high input impedance are well-suited for measuring extremely small static charges. However, integrating them into custom circuits involves considerable cost and requires specific conditions. In contrast, charge amplifiers feature a low input impedance suitable for the measurement of moderately small charge flows in dynamic applications. We demonstrated their exceptional sensitivity with ferroelectret sensors in our force myography setup, enabling the detection of volumetric muscle contractions in the human forearm for gesture recognition [54]. Within walking scenarios, the full body weight acts on the air cavities and generates a charge flow resulting in comparatively large amplitudes. Therefore, in the current scenario, we choose to measure the voltage across a large value shunt load using a low-cost and less complex terminal stage to amplify the sensor output voltage for impedance matching. Accordingly, this results in a less sensitive circuit than the charge amplifier but with increased dynamic range and the ability to suppress drift.

We employ shielded twinaxial cables for the connection between each sensor and the measurement board to ensure a high signal-to-noise ratio (SNR). The board housing is 3D-printed from PLA and is fit with an elastic strap above

the hip of the participant. This leaves the option to add force myography sensors to the leg muscles in further studies and enhances wearer comfort by eliminating any disturbance to the walking experience caused by devices attached to the ankle.

The output voltage of each sensor is captured using our battery-powered measurement board, which comprises an analog matching stage for each channel, an analog-to-digital converter (ADC), and a microcontroller facilitating wireless connectivity to the acquisition PC. The measurement circuit is designed to match the analog sensor behavior to the ADC (MCP3008, Microchip Technology, Chandler, AZ, USA) input range and adjust the sensor impedance. As the underlying piezoelectric effect primarily induces dynamic responses, we use capacitors as DC blockers, mitigating offset drift, and resistors to bias the alternating sensor signal with a constant offset based on our previous circuit [63]. While the sensor's capacity establishes an intrinsic high-pass characteristic with the load [70], the circuit's input impedance is adjusted to further raise the cut-off frequency, thereby, enhancing drift suppression. The ADC samples the four matched and filtered sensor signals (500 Hz, 10 bits). A microcontroller ESP32 (HUZ-ZAH32, Adafruit Industries, New York City, NY, USA) reads from the ADC through the Serial Peripheral Interface (SPI) and accumulates this data along with timestamps in packets.

We use the User Datagram Protocol (UDP) with an update rate of 100 Hz to transfer the data chunks between the multi-threaded ESP32 and the acquisition PC. A dedicated router (TL-WR902AC, TP-Link, Hong Kong) in infrastructure mode is set up for the wireless connection to the ESP32 and the wired connection to the PC to overcome connectivity issues, which happen irregularly if the ESP32 and the PC communicate directly. As a result of this setup and configuration, we achieve zero packet loss throughout all of our experiments. Essentially, our system is designed as a fully autonomous platform for gait analysis, enabling the application in daily life, which is not feasible with stationary equipment such as an instrumented treadmill.

Our cross-platform software is built on Python 3 with a Qt graphical user interface and uses a UDP socket to receive the data stream from the ESP32. A live plot for each sensor channel provides an intuitive way to initially verify the incoming sensor data. The data are then saved in text-based files for further processing.

We conduct a latency characterization of the sensor system to verify the fast dynamic response of the ferroelectret sensor system. Employing the built electronics, we temporarily select a maximum sampling rate of 200 kHz for the ADC to handle the sensor input. Additionally, the microcontroller is programmed to turn on an LED when the sensor signal crosses a threshold slightly above the idle state. This setup allows for visual confirmation of the activation and facilitates the system's characterization. A 100 g weight is vertically dropped five times onto the sensor from a height of 5 cm using a linear guide. The experiment is recorded using a high-speed camera (Chronos 1.4 model CH14-1.0-32C, Kron Technologies, Eastlake, BC, Canada) with the maximum available frame rate of 40.414 kHz to determine the time of initial contact. After the weight touches the sensor surface, the LED turns on with a

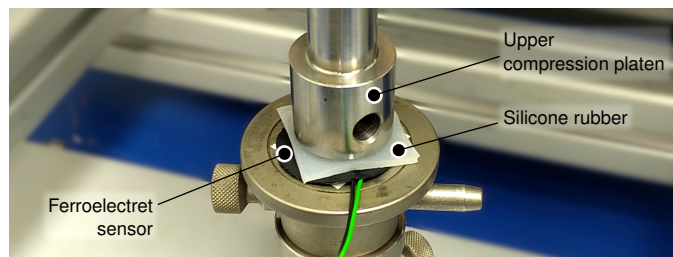


**Fig. 2.** A single sensor, of which the insole comprises four, is under test to facilitate a seamless integration into the universal testing machine. The upper compression platen has a slightly smaller diameter than the ferroelectret sensor and is positioned with some distance to it before the trial. With the insert of silicone rubber, we model an interface change similar to human tissue.

delay of  $0.466 \text{ ms} \pm 0.264 \text{ ms}$ . The delay is significantly below the typical sensor acquisition rate, thereby, sufficiently small for our measurements.

### C. Sensor Characterization

We aim to characterize our sensors with a procedure that is reproducible, automated, and closely resembles the rapid weight transfers during human locomotion. Therefore, a universal testing machine (Inspekt table 5 kN, Hegewald & Peschke, Nossen, Germany) serves as tool for the sensor characterization (Fig. 2), situated in a laboratory under controlled temperature of  $22^\circ\text{C}$ . We employ a loading procedure in position-control mode to optimize the velocity of the testing machine and satisfy the dynamic testing capabilities with large static forces that are required for the insole application. The forces of up to 800 N on a single sensor exceed the expected measurement range under the human foot sole at the sensor area.

Due to the flexibility and larger size of the insole compared to the platens of the universal testing machine, we employ several isolated ferroelectret sensors to seamlessly integrate them into the testing machine setup. One sensor at a time is affixed to the lower platen of the testing machine with adhesive tape. A compression platen of diameter 28 mm is mounted to the upper part of the machine to accommodate the sensor's diameter of 28 mm. Each examination begins with the compression platen slowly ( $0.01 \text{ mm s}^{-1}$ ) approaching the sensor from the top. A force of 0.1 N establishes initial contact and marks the beginning of the test protocol. One test cycle comprises a gradual increase in force with a fixed slope up to the predetermined maximum, a phase of sustained force application, and a controlled decrease in force returning back to zero. Multiple cycles with a varying number of repetitions are used to characterize the sensor's electromechanical properties including sensitivity, measurement range, hysteresis, repeatability, and drift. Since the differences between the three tested sensors are minimal ( $<2.5\%$  maximum deviation) and fall within the expected tolerances of the manual manufacturing process, we present the results for one sensor only in the following to ease understanding.

1) **Sensitivity and Measurement Range:** Sensitivity and linearity are fundamental aspects of a sensor's performance. Increased sensitivity results in a larger sensor output for the

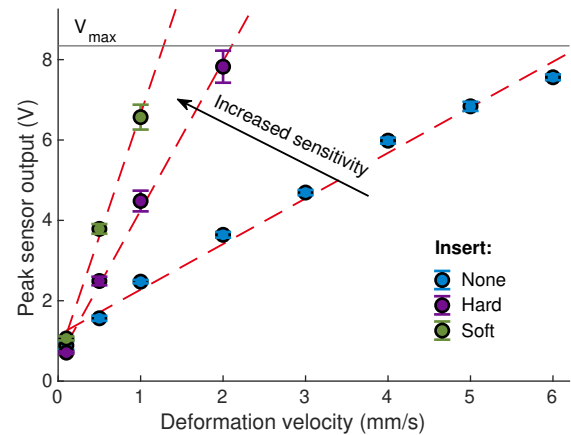


**Fig. 3.** Peak sensor output over the deformation velocity measured as voltage drop over a large value shunt load, respectively for three different interfacial materials used for the cyclic loading procedure. The characteristic demonstrates a highly linear ( $R^2 > 98.80\%$ ) response for all scenarios. Inserting silicone rubber that is of similar viscoelasticity as human tissue, increases the sensitivity compared to directly loading the sensor with a metallic compression platen. Moreover, the electronic circuit causes a clipping for voltages beyond the upper limitation  $V_{\max}$ , which is adjusted for the expected input signal range, thereby, extending the measurement range for harder interface materials.

same measured quantity. However, an elevated sensitivity leads to a reduced measurement range under otherwise constant configuration. A linear sensor characteristic is desirable to ensure a constant sensitivity and resolution across the entire measurement range without requiring an adaptive gain. This not only reduces the demands on electronics but significantly simplifies the calibration and facilitates embedded data processing. The linearity is compared using the coefficient of determination  $R^2$ .

We assess the sensor's performance using various interfacial materials, including 1-mm-thick silicone rubber disks that have the same size as the sensor and similar viscoelasticity as human tissue. The silicone rubber disks of different elasticity are placed as an insert between the metallic compression platen and the sensor to model an interface change (Fig. 2). Considering the dynamic nature of human gait, we regard the deformation velocity as a significant parameter for gait measurements. Therefore, we define the sensitivity of the sensor output with respect to the deformation velocity. The peak sensor amplitude is acquired over a large value shunt load using our measurement board while repeating the loading procedure ten times for each deformation velocity and insert configuration.

The sensor sensitivity and measurement range highly depend on the viscoelasticity of the interfacial material, thus, the peak amplitude depends on the deformation velocity (Fig. 3). The utilization of soft silicone rubber (Ecoflex 00-35, Smooth-On, Macungie, PA, USA) results in the highest sensitivity of  $6.10 \text{ V mm}^{-1} \text{ s}$ . With the use of hard silicone rubber (Dragonskin 10, Smooth-On), the sensitivity diminishes to  $3.71 \text{ V mm}^{-1} \text{ s}$  and further reduces to  $1.14 \text{ V mm}^{-1} \text{ s}$  without any material between the sensor and the metallic compression platen. The large viscoelasticity of soft silicone rubber correlates with a large sensor sensitivity. Moreover, the potential

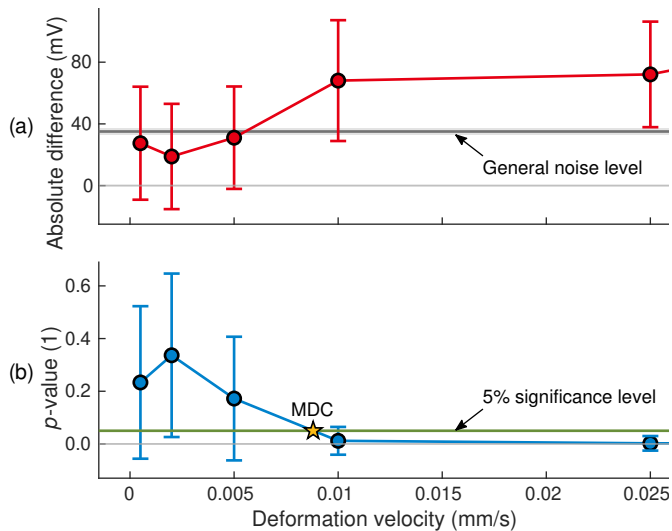


Fig. 4. The sensor's minimal detectable change (MDC) in deformation velocity depends on the significant difference between loaded and unloaded sensor output. (a) The absolute difference with the corresponding general noise level calculated from the randomized signal samples. (b) The  $p$ -value from an unpaired-sample Student's  $t$ -test with the decision relevant 5% level over the deformation velocity used during loading. The MDC lies in-between two of these measured values and is determined with a piecewise linear regression.

measurement range expands when using harder interface materials due to the maximum input voltage  $V_{\max}$  clipping all values above. The upper limit is determined by the electronic circuit design intended to maximize resolution without causing signal clipping within the expected input signal range in the insole application.

The peak sensor output to deformation velocity characteristic demonstrates a highly linear response across all scenarios: with soft silicone rubber ( $R^2 = 99.66\%$ ), with hard silicone rubber ( $R^2 = 99.56\%$ ), and without silicone rubber ( $R^2 = 98.80\%$ ). As found in our preceding work [64], the raise in sensitivity is a result of the soft silicone rubber penetrating the grid spaces within the sensor structure, which results in a larger deformation and a larger sensor output. Within the application of the ferroelectret insole, the sensor interfaces with the human foot sole. Consequently, this results in a dependency of the absolute sensor amplitude on individual foot sole stiffness and viscoelastic properties, which can differ from one person to another [67]. Despite these dependencies, if necessary, a single linear factor can adequately correct the absolute sensor output to account for these individual variations in foot sole properties.

In conclusion, when applied practically, it becomes imperative to tailor the voltage range to align with the anticipated measurement range for the deformation velocity. Such a calibration can be achieved through walking experiments and can increase the sensitivity at the cost of a reduced measurement range. The linear relation of sensor output and deformation velocity makes the ferroelectret sensor well-suited for practical use.

2) **Minimal Detectable Change:** We assume that the minimal detectable change (MDC) in deformation velocity can be determined experimentally and is characterized by the point

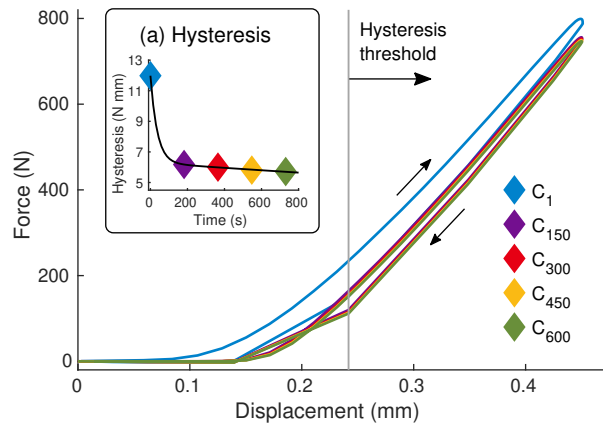
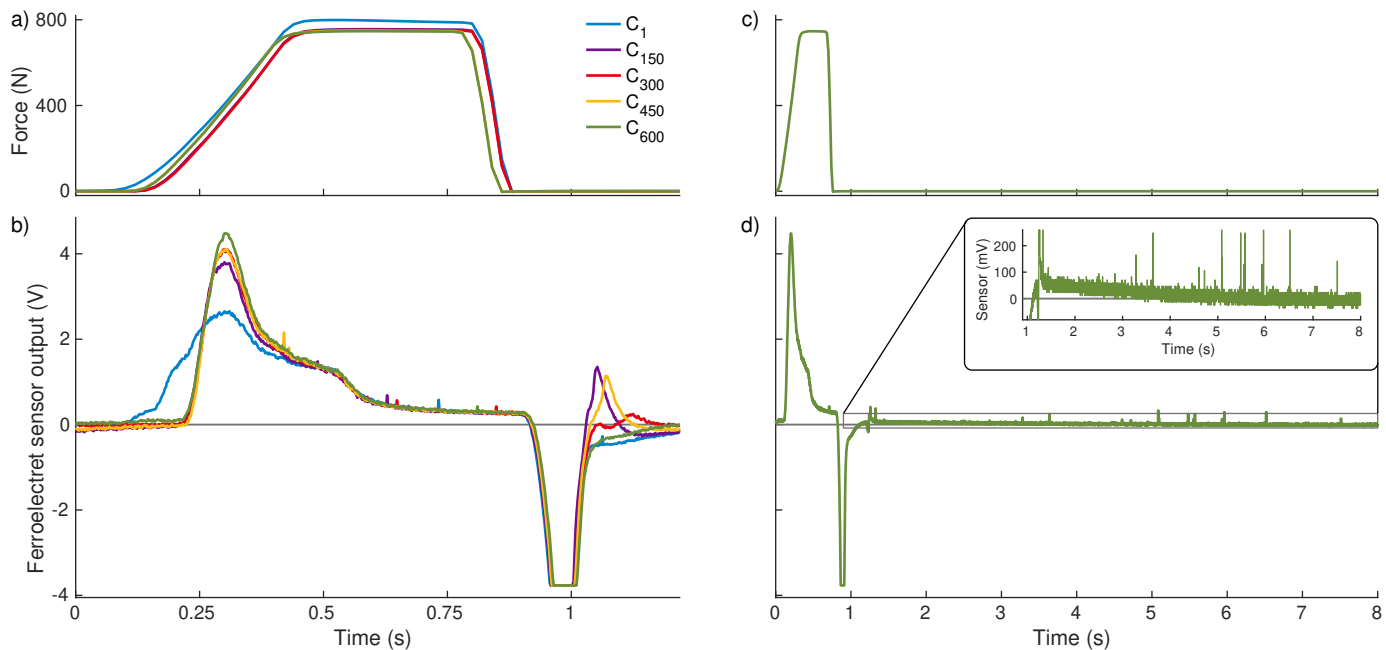


Fig. 5. Test machine force over sensor displacement for five specific load cycles ( $C_1$  to  $C_{600}$ ) during a continuous procedure with 600 load cycles up to 800 N, each followed by a release back to zero with a cycle time of about 1.1 s. The hysteresis effect is calculated from the areas enclosed by the hysteresis threshold to the left and the five cycle plots to the right, respectively. Below this threshold (0.242 mm), the resolution of the testing machine force is too low due to the fast loading with no more than 50 Hz sampling. (a) The hysteresis effect declines with ongoing cyclic loading and levels out, which is a typical behavior for viscoelastic materials, such as the PLA polymer used.

where we identify a significant difference between a sensor in loaded condition and without load. The determination of MDC uses samples corresponding to the two conditions: 1000 without any load and 1000 with the sensor subject to a constant velocity. We extract randomized signal samples of 10 ms from ten cycles lasting up to 15 min. The sample length of 10 ms complies with an often used controller update rate for exoskeletons [71]. The procedure is repeated for the selected velocities: 0.0005, 0.002, 0.005, 0.01, and 0.025  $\text{mm s}^{-1}$ . We use an unpaired-sample Student's  $t$ -test for each of the 1000 comparisons to confirm a significant difference in between loaded condition and without load, after confirming a normal distribution using the Shapiro-Wilk test. Subsequently, means and standard deviations of the  $p$ -values are determined. MDC is finally defined as the intersection between the 0.05 significance level and the piecewise linear regression connecting the discrete  $p$ -values for the measured deformation velocities (Fig. 4).

For a better interpretation of the results, the general noise level of our sensor is determined as such that the signal noise corresponds to the standard deviation of the signal at an equal deformation velocity. Thereafter, we average the signal noise of all the ten repetitions with and without load for all the deformation velocities to determine the general noise level. The sample noise values are on average slightly larger (3.65%) for the loaded condition compared to the condition without load. The resulting general noise level is  $40.26 \text{ mV} \pm 3.43 \text{ mV}$ .

With a velocity larger than 0.01  $\text{mm s}^{-1}$ , the signal level between with and without load conditions is clearly distinguishable ( $p = 0.0118 \pm 0.0527$ ), while the mean of absolute difference ( $68.06 \text{ mV} \pm 40.26 \text{ mV}$ ) exceeds the general noise level (Fig. 4). With a velocity smaller than 0.005  $\text{mm s}^{-1}$ , we are unable to differentiate with and without load conditions ( $p = 0.1722 \pm 0.2347$ ) and the mean absolute difference ( $31.05 \text{ mV} \pm 33.30 \text{ mV}$ ) drops below the general noise



**Fig. 6.** Five selected equidistant load cycles ( $C_1$  to  $C_{600}$ ) from a repetitive loading procedure with similar properties to the human gait regarding force slope and stride frequency. (a-b) Once the force settles at its maximum (time 0.55 s), the sensor signal levels off but keeps a positive offset of similar height across all cycles. (c-d) After the last signal drop during  $C_{600}$ , the curve decays slowly and eventually levels off at zero 6 s later.

level. The interpolated MDC for the deformation velocity of  $0.0088 \text{ mm s}^{-1}$  lies in between these two conditions. Even for the softest evaluated silicone rubber, this MDC corresponds to only about 1% of the measurement range adjusted for our application. We expect that such a small MDC is relevant for deformation velocities found in more sensitive applications such as force myography [54]. In conclusion, the MDC of our sensor does not interfere with our application for detecting force changes using an insole during human walking.

**3) Hysteresis:** Ferroelectrets are made from polymers, which are viscoelastic materials and typically display a substantial time dependence in their mechanical properties, such as creep due to static stress and hysteresis within cyclic loading conditions [72]. We assess the magnitude of the hysteresis within our sensors and track its temporal evolution across an increasing number of load cycles. We employ a position-controlled loading procedure to optimize the testing machine's velocity. This approach is crucial for replicating a loading profile akin to human gait regarding stride frequency and the large force slope. Our protocol involves 600 loading cycles up to 800 N each, followed by a release back to zero. Our methodology closely simulates the rapid weight transfers during a gait cycle. The cycle duration of approximately  $1.1 \text{ s}$  corresponds to a walking speed of  $1.3 \text{ m s}^{-1}$ . We employ this identical protocol for both the full-scale and zero drift assessment. The hysteresis calculation entails measuring the areas between the hysteresis threshold set at  $0.242 \text{ mm}$  and the five selected, equidistant cycle plots  $C_1$  to  $C_{600}$ , respectively (Fig. 5). Below this threshold, the testing machine lacks sufficient resolution due to the restricted sampling frequency of  $50 \text{ Hz}$ .

Approximately, loading requires 300 ms, holding force 350 ms, unloading 100 ms, and resting 350 ms. On the loading path, the force exceeds that of the unloading at equivalent

displacement (Fig. 5). The hysteresis effect demonstrates an exponential decrease with continuous cyclic loading and eventually stabilizes (Fig. 5a). The increased force required during the loading phase for an equivalent displacement indicates a viscoelastic deformation that persists within the sensor material across multiple repetitions, which is a characteristic of viscoelastic materials such as polymers used in ferroelectrets [72]. In conclusion, as the hysteresis diminishes over the first 200 s, for the application of the insole, especially absolute values of early load cycles shall be either disregarded or approached with caution.

**4) Zero Drift:** If the sensor output varies, even without a change in the measured variable, a zero drift is present. This phenomenon influences the performance of prolonged sensor use, necessitating regular recalibration. We employ the same five equidistant load cycles ( $C_1$  to  $C_{600}$ ) previously used for the hysteresis characterization (Fig. 5) to evaluate the zero drift and synchronize the data from all cycles at the ferroelectret sensor maxima. Although ferroelectret sensors commonly display inherent mechanical drift, akin to most polymers, we anticipate compensation for this drift through our analog electronics. Our approach involves high-pass filtering of the sensor signal, effectively eliminating the drift.

Given our use of position-controlled loading, the force amplitude during  $C_1$  is slightly larger compared to the other evaluated load cycles, while the sensor amplitude exhibits a smaller yet broader peak (Fig. 6a-b). Once the force stabilizes at its maximum (time 0.5 s), the sensor signal plateaus, maintaining a positive offset of approximately 300 mV on average (around time 0.75 s), which is about 10% of the signal amplitude for the first loading cycle. This offset remains relatively consistent across the five selected cycles and reverses upon unloading. During unloading, the sensor signal experiences negative clip-

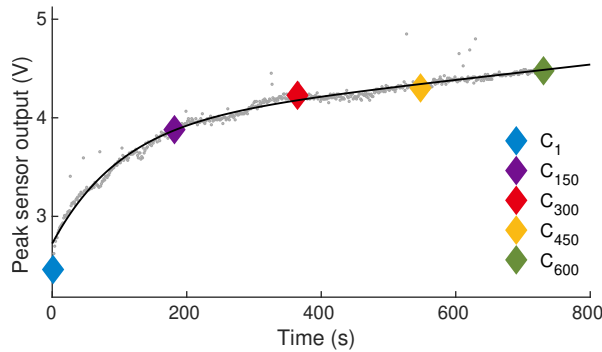


**Fig. 7.** The peak sensor output during rising load is extracted to approximate the full-scale drift over 600 cycles up to 800 N with the same five equidistant load cycles ( $C_1$  to  $C_{600}$ ) highlighted as in Figs. 5 and 6. The exponential drift diminishes over the first 200 s and the sensor output continues to increase approximately linearly with 0.61 mV per cycle over the measurement duration.

ping due to the rapid reduction in the testing machine's force. Following the final signal drop in  $C_{600}$ , the sensor amplitude gradually diminishes and eventually stabilizes at zero after approximately 6 s (Fig. 6c-d). We observe a similar evolution towards zero during the rest phases without any mechanical load, although a complete reset is unachievable due to the short break before the subsequent loading begins.

As the measurement is free of any zero drift, we assume that our analog electronics effectively compensates for the inherent material drift. Under constant load, the sensor output is expected to remain at zero, due to the absence of a deformation velocity. However, an offset from zero that remains for up to 6 s (Fig. 6d) is found. Additionally, the amplitude of the offset is consistent regardless of the number of previous cycles underscoring a reliance of the amplitude on the actual deformation rather than the deformation velocity. The signal returning to zero after the completion of the final load cycle  $C_{600}$  can be explained by a mechanical restoring process, potentially associated with viscoelastic relaxation, as well as by an electrical discharge process. In conclusion, we observe a zero offset, when load is applied, rather than a zero drift (Fig. 6b). The magnitude of the offset is sufficiently small, ensuring that our system aligns with the requirements for accurately detecting gait events in the insole application.

**5) Full-scale Drift:** In contrast to the zero drift, full-scale drift refers to a shift in the output close to the maximum amplitude or a modification of the upper measurement limit. For analysis, the experimental data from the hysteresis evaluation are used. The peaks of the sensor output are extracted and utilized to estimate the full-scale drift by an exponential fit. The results indicate the presence of a full-scale drift for continuous loading cycles (Fig. 7). Although the full-scale drift diminishes over the first 200 s, the sensor output continues to increase over the end of our measurement protocol (12 min) at a rate of approximately 0.61 mV per cycle. However, the experiments on the repeatability showed complete relaxation of the full-scale drift if breaks of 60 to 120 s are made in between loading cycles. The drift primarily arises from the mechanical creep within the sensor structure. Consequently, we expect an absolute saturation of the drift over extended

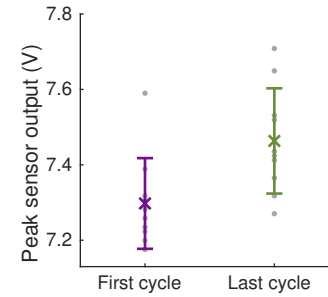


**Fig. 8.** The sensor undergoes ten iterations, each comprising ten consecutive loading cycles, with a break in between cycles and extended breaks in between iterations. The peak sensor output from the last cycle compared to the first cycle of each iteration slightly increases, attributed to the full-scale drift, whereas both exhibit similar variability. This not only showcases the overall repeatability of the sensor output but also verifies its viscoelastic behavior.

measurement times, even though the drift per cycle at the end of our protocol is already low. Young adults typically walk about 6500 steps a day [73], which will result in a drift of approximately 1.8 V at each insole sensor, assuming the worst-case scenario of continuous walking without a break and no additional saturation of the drift rate. With the present amplifier tuning, this still falls well within the available input range. Thus, an event detection such as in the gait scenario remains unaffected. Based on this finding, in applications involving continuous loading cycles without breaks, the design of the voltage range needs to account for such a drift. In conclusion, the application of our insole sensors for gait event detection is possible, assuming proper consideration for the potential full-scale drift within the layout of the electronics.

**6) Repeatability:** The analysis of the hysteresis revealed a characteristic viscoelastic behavior influenced by prior loading conditions. Based on literature [72], we posit that relaxation not only relies on prior loading but also on time. Consequently, we conduct multiple repetitions using the same cyclic loading procedure to assess the repeatability of the sensor output. The sensor undergoes ten iterations, each comprising ten loading cycles up to 700 N with a deformation velocity of  $5 \text{ mm s}^{-1}$  and a break of 60 s in between cycles. In between iterations, we extend the break to 120 s to facilitate the relaxation of the viscoelastic material. We assess the variability of the first and last loading cycles using Levene's test.

On average, the peak voltage output in the last load cycle (7.47 V) shows a slight increase of 1.8% compared to the first load cycle (7.31 V), attributed to the full-scale drift (Fig. 8). While evaluating this sensor characteristic, the absolute voltage amplitude is found to be larger compared to others due to the correlation with the increased deformation velocity. Notably, the last and the first cycles exhibit similar variability ( $p > 0.05$ ) with standard deviations of 1.9% ( $\pm 0.139 \text{ V}$ ) and 1.6% ( $\pm 0.120 \text{ V}$ ) of the peak outputs, respectively. Results show that the first and the last repetition are quite stable across the ten iterations, which proves sensor repeatability. However, breaks of 60 s in between loading cycles are not sufficient to completely relax the viscoelastic polymer material within each iteration. In contrast, breaks of 120 s in between iterations prove to be effective in achieving



almost complete relaxation. In conclusion, the ferroelectret sensors provide a similar output for a similar loading behavior while breaks will impact the absolute level of voltage output. Nevertheless, the detection of voltage peaks, which is crucial for our event detection, remains robust against changes in absolute magnitude.

### III. APPLICATION IN GAIT ANALYSIS

The previously investigated ferroelectret sensors feature a dynamic sensor principle that reveals a highly linear sensor characteristic in our statistical evaluation. Accordingly, we emphasize their application as a proof-of-concept in dynamic contexts such as walking. Four sensors are arranged in an insole array to assess their collective performance for event detection in gait analysis, a crucial aspect of biomechanical research and wearable robotics control.

#### A. Insole Design and Preparation

The insole is manufactured similarly to the previously characterized single sensor element, extending the three main pressure areas [29] with a toe sensor to detect the last contact during toe-off. The four sensors increase the spatial resolution across the entire sole area as a proof-of-concept while restraining the assembly effort as well as the complexity of wiring and electronics. We print the insole comprising the sensors in one piece using the same layer stack as for the single sensors [64]. In contrast to the single sensors, the insole features several seamless layers that firmly secure the sensors in place. In particular, both PLA films and textile covers span the entire sole area, eventually, forming the foot shape.

Each individual sensor element is separately wired and treated electrically to turn it into a ferroelectret. The functionality of each individual sensor is confirmed by promptly lifting a weight via a vertical linear guide away from the sensor and reviewing its outputs.

#### B. Experimental Setup

The experimental setup includes our insole with four ferroelectret sensors placed under the calcaneus (heel), the fifth metatarsal head at the lateral forefoot (LF), the first metatarsal head at the medial forefoot (MF), and the hallux (toe). Furthermore, we employ the built measurement board connected to the insole and an instrumented treadmill (ADAL 3D, HEF Tecmachines, Andrézieux-Bouthéon, France) that is typically used to reliably assess walking GRFs (Fig. 9). The instrumented treadmill offers trigger outputs at the instrumentation amplifier, which differ in length, indicating the start (2.3 ms) and end (0.4 ms) of the GRF acquisition. We connect a coaxial cable from the treadmill's instrumentation amplifier to our measurement board and use the hardware interrupts on the ESP32 to detect the incoming trigger edges. The trigger signal is used to synchronize the GRF with the insole data in our software. We place the insole on the treadmill surface and drop a weight on both to test the synchronization. No delay of either system beyond the sampling time of the GRF (4 ms) is observed.

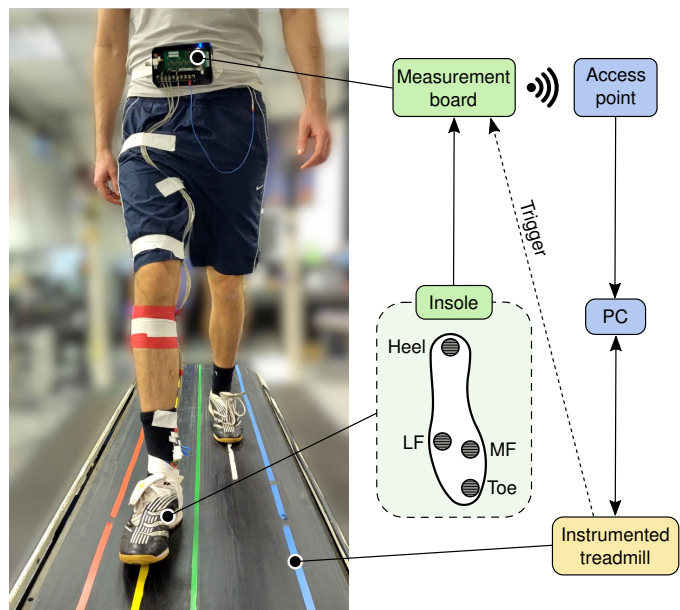


Fig. 9. The autonomous ferroelectret insole system is examined with one participant on an instrumented treadmill as a reference regarding gait event detection. A trigger line ensures the synchronization between both systems for this experiment. Data from the sensors placed under heel, lateral forefoot (LF), medial forefoot (MF), and big toe are assessed for on average 100 strides across five different walking speeds.

#### C. Experimental Protocol

The setup is extensively tested with one participant (male, 31 years, 176 cm, 69 kg) without gait related impairments, who wears the insole in the right shoe (EU size 43). The study received approval from the Ethics Committee of Technische Universität Darmstadt and is conducted in accordance with the principles outlined in the Declaration of Helsinki. The participant provided written informed consent. We specify five different walking speeds (50%, 75%, 100%, 125%, 150%) derived from the nominal walking speed (100%,  $1.3 \text{ m s}^{-1}$ ), which are controlled by the treadmill resulting in belt speeds  $v_{50}$  to  $v_{150}$ . We begin with a 200-second preconditioning phase to stabilize the sensor output (Fig. 7) and continue with the measurement protocol that consists of a two-minute walking period at each speed, starting with the slowest speed  $v_{50}$ . Afterwards, we analyze phases of constant speed, which contain 74 to 124 strides depending on the speed.

#### D. Data Analyses

The data analyses are carried out in MATLAB (2022b, MathWorks, Natick, MA, USA). We offer the preprocessed structured data for free use in HDF5 format along with sample scripts for MATLAB and Python under license CC-BY [74]. The sensor data from the insole are high-pass filtered with a cut-off frequency of 0.1 Hz and low-pass filtered with 20 Hz using a second order Butterworth filter design. The treadmill data are low-pass filtered using the same parameters. We linearly interpolate the measurements from the instrumented treadmill (240 Hz) to match the sensor data sampling frequency (500 Hz) and timestamps. The strides are segmented using the treadmill data from one heel strike (0% of the stride)

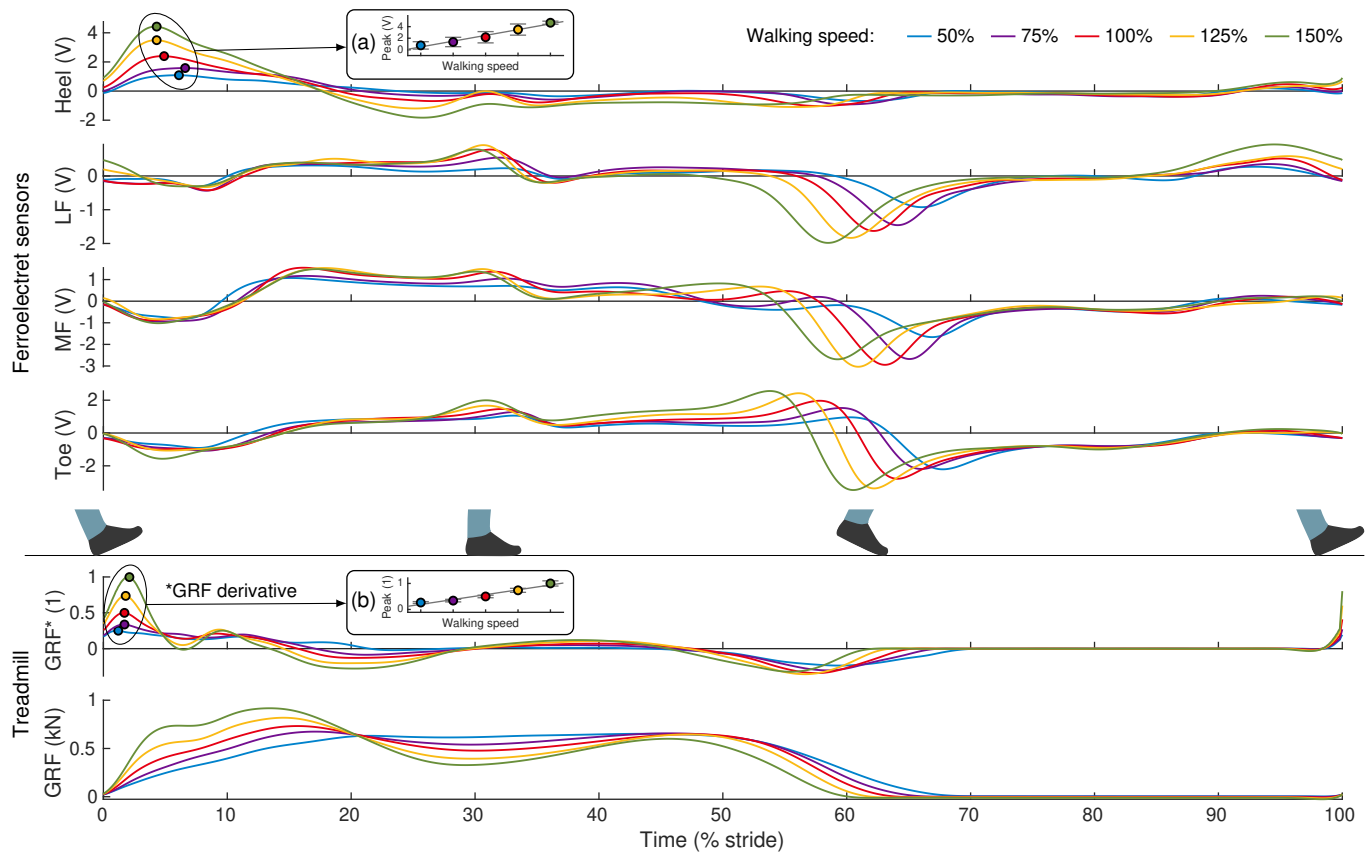


**Fig. 10.** Mean of the individual insole sensor outputs, placed on heel, lateral forefoot (LF), medial forefoot (MF), and big toe, along with the vertical ground reaction force (GRF) from the instrumented treadmill across five different walking speeds ranging from 50% to 150% of the nominal walking speed (100%,  $1.3 \text{ m s}^{-1}$ ). The strides are segmented from one heel strike (0% of the stride), when the vertical GRF component of the right foot exceeds 20 N, to the following heel strike (100%) of the same foot in order to normalize the stride time. The stance phase ends with the toe-off event (around 60%), which coincides with the minimum of the toe sensor signal. A relative shortening of the stance phase with increased walking speed is extracted from the ferroelectret sensor data as well as from the treadmill data. (a) The heel sensor peak during initial contact (around 5%) scales linearly with the walking speed. (b) The same applies for the normalized GRF derivative.

to the subsequent heel strike of the same leg (100%) in order to normalize the stride time. The heel strikes are identified when the vertical GRF component of the right foot exceeds a threshold of 20 N. The height of the threshold holds a crucial role when detecting heel strike and toe-off events during the gait cycle and is selected to be just above the noise level of the treadmill data [17]. We calculate the arithmetic mean for each sensor across all strides at one speed to visualize the average stride in a comprehensible format. Additionally, we compute the GRF derivative with respect to the relative stride time and normalize it to the maximum value to enable the validation of the electromechanical behavior derived in (3).

Furthermore, we proved a dependency of the sensor output on the cover material (Fig. 3) and the cover thickness in a previous publication [64]. As a result, the system signal relies on the properties of the contact surface, thus, on the individual's foot sole. Recognizing that an absolute threshold overlooks these variations, we establish the threshold for heel strike detection relative to the peak amplitude of the preceding stride (at 15%). We select the heel sensor in the insole for the heel strike detection as it establishes contact to the ground first. The toe sensor as last foot contact is utilized to detect the foot lift. A negative deformation velocity on the sensors causes

a negative sensor peak due to the sensor polarity applied. Therefore, the toe-off event is observed with a negative peak detection at the toe sensor, after the output falls below an absolute threshold of 1.75 V to avoid erroneous triggering.

The time difference in gait event detection involves comparing the timings of the ferroelectret sensors (heel and toe) to the GRF of the treadmill across the five different speeds. The treadmill measurement serves as the ground truth. The time difference is negative if the ferroelectret sensor based thresholding results in an earlier detection against the corresponding event derived from the treadmill measurement. A later detection gives positive values. Individually for each event in time, the time difference is calculated as absolute value and relative to the mean stride duration to adjust for the dependence on the walking speed. Separately for each speed, we determine the statistical significance of the difference in means between the two data sources for the event detection from a Wilcoxon signed-rank test, after identifying slight deviations from a normal distribution. Subsequently, the mean and standard deviation are derived across all heel strike and all toe-off events, respectively.

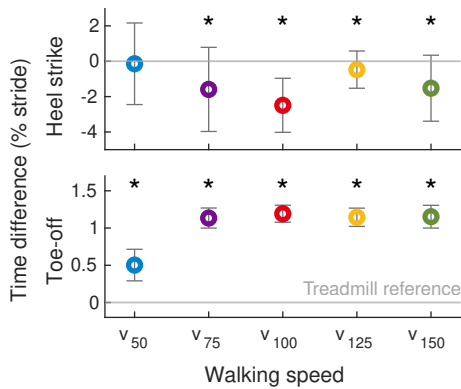


**Fig. 11.** Differences in stride time for the gait event detection based on the insole's ferroelectret sensor output (heel and toe) compared to the vertical ground reaction force (GRF) of the instrumented treadmill as ground truth (0%). If the ferroelectret sensor based thresholding results in an earlier detection against the corresponding GRF event, the time difference is negative; a later detection gives positive values. Walking speeds are controlled by the treadmill belt from slowest  $v_{50}$  to fastest  $v_{150}$ . The heel strike is recognized significantly earlier with our sensors compared to the GRF for all walking speeds but  $v_{50}$ . Toe-off is detected with low variation. Note the different axes scaling. Asterisks denote a statistically significant difference from the ground truth ( $p < 0.05$ ).

### E. Experimental Validation

During the experiment, the mean outputs of the ferroelectret sensors, positioned under the heel, LF, MF, and toe, change in amplitude along with the vertical GRF from the treadmill across the five walking speeds (Fig. 10). All signals show characteristic peaks within the stride. During the loading response, we find a strong positive peak for the heel sensor and small negative peaks for the LF, MF, and toe sensor. During mid-stance, a small signal increase with minor fluctuations occurs throughout all sensors. During lift-off, a large negative peak is found. The derivative of the vertical GRF component, which directly relates to the ferroelectret's output according to the electromechanical behavior derived in (3), shows similar distinct peaks for loading and lift-off phase. A low average variability of 192 mV (standard deviation) is found across the entire stride for all speeds, which corresponds to 7% of the average peak height during loading response, underscoring the repeatability of the sensor measurements.

1) *Loading Response:* The loading response results in a positive peak of the treadmill's GRF derivative, which scales linearly ( $R^2 > 95.80\%$ ) with the walking speed (Fig. 10b). The positive peak of the heel ferroelectret sensor shows a similar linear ( $R^2 > 97.74\%$ ) scaling over the walking speed (Fig. 10a). Using the positive slope of the heel sensor towards this peak seems reasonable for the heel strike detection. A threshold of 15% of the preceding peak is selected for triggering the event detection reliably for all analyzed strides at all speeds. When comparing the detection based on the ferroelectret sensors to the GRF, we recognize the heel strike to occur significantly ( $p < 10^{-5}$ ) earlier (16.2 ms  $\pm$  9.5 ms) with our sensorized insole for all walking speeds except the slowest  $v_{50}$  (Fig. 11).

2) *Mid-stance:* During mid-stance the load shifts from the heel towards the forefoot [16], which results in negative amplitudes for the heel and positive amplitudes for the forefoot sensors (Fig. 10). Before mid-stance (around 10% of the

stride), a zero crossing from negative to positive takes place for the forefoot sensors LF, MF, and toe, where the timings align with the placement in the insole. Earlier timings occur for posterior placement. A similar behavior is found after mid-stance, where the zero crossing from positive to negative aligns with the same order. In combination with the distinct peaks and timing of peaks for the heel and toe sensor, this indicates a possibility to resemble the pressure distribution and the center of pressure (CoP) trajectory during the stride. Similar to our findings, largest pressure amplitudes are found for the heel and toe sensor, while relatively smaller peaks are found for the sensors covering the ball of the foot [75]. The trajectory of the CoP during walking [15] aligns with the shift from posterior to anterior loading found for our insole. Prior research indicates that the CoP can be derived from three pressure sensors employing an anatomical foot model [29]. Furthermore, it will be beneficial to detect intermediate events such as the flat-foot and heel-off, similar to the recent progress in IMU-based gait segmentation [19]. We posit that future investigations consider an analysis of the pressure distribution along with a similar CoP calculation using our insole sensors. In line with the estimation of the CoP, possible further investigations involve the determination of the vertical GRF by the integration of a weighted sum of all insole sensor outputs. This can be accompanied by an increase in spatial resolution using a sensor matrix with smaller elements, which is easily possible through the 3D-printed design.

3) *Lift-off:* During lift-off, while the heel sensor returns from negative to zero, the forefoot sensors show highly negative outputs, caused by the decrease in load. This characteristic is consistent with the negative amplitude of the force derivative and scales with walking speed. These global minima, occurring in between 60% to 68% of the stride depending on walking speed, coincide with the respective toe-off event timings determined by the GRF. Similar to the zero crossings before mid-stance, the timing order of the peaks aligns with the sagittal placement on the insole. Furthermore, the shift of load from the ball of the foot to the toes is evident through positive peaks in the toe sensor shortly before toe-off. These peaks scale with walking speed and reach up to 2 V. Both the order in timing and the shift in load strengthen the idea of using insole data to estimate the CoP movement. In addition, a detection of the toe-off timing in combination with the detected walking speed, extracted from the ferroelectret sensors, enables the identification of spatio-temporal characteristics, including stance and swing time, as well as stride length [18].

4) *Gait Event Detection:* Heel strike and toe-off events are detected in a reasonable range with a maximum difference of up to 2% of the stride time (Fig. 11). While heel strike detection is slightly earlier, toe-off detection is slightly later. Toe-off detection occurs reliably about 1% of the stride time after the treadmill signal crosses the threshold with low variation across all speeds. For reference, a change of 4% in the timing for peak assistance in a hip exoskeleton did not significantly impact metabolic cost, whereas a change of 8% did [76]. The heel strike is detected based on a threshold relative to the positive peak of the heel sensor of the previous stride. This threshold can be easily adapted to change the detection timing.

While the toe-off detection uses the negative peak of the toe sensor, a similar adaptation to the corresponding threshold, as done for the heel strike, can further improve the slightly late timings.

With the current approach, we detect the heel strike earlier (about 16 ms) than the reference from force measurement plates. In addition, this is faster than the commercial insole F-scan, which shows a mean delay of 22 ms to the reference, even with an improved detection method [21] as well as other custom-built insoles such as GaitShoe (on average 6 ms earlier [33]) with various sensor technologies, such as piezoelectric and piezoresistive sensors, as well as IMUs. Accelerometers, as built into IMUs, show similar tendencies with on average slightly earlier (11 ms) heel strike and slightly later (19 ms) toe-off events, even though the deviations from the foot switch reference utilized are not significant [77]. While an earlier detection timing can be of advantage in wearable robotics to provide an additional buffer time for the controller, a later timing will be of disadvantage as the assistance is applied too late [9]. Even though the often used F-Scan system generates late responses for the heel strike and early responses for the toe-off events, literature suggests that an adaptation of the thresholds can improve detection timings [21]. This holds true for our system, as the threshold based approach allows, if required, to shift the heel strike timings to later and the toe-off timings to earlier points to match the GRF-based timings. Further analysis may also consider advanced algorithms in the time-frequency domain [78]. Future research needs to show if the detection approach is applicable to people with pathological gait and other kind of daily movements, such as stair ambulation or walking inclines.

#### IV. CONCLUSIONS AND FUTURE WORK

In this work, we engineered a customized insole with four ferroelectret sensors, all 3D-printed monolithically from polylactic acid (PLA). We aimed at using the insole for human gait phase detection based on the events of heel strike and toe-off to extract control inputs for lower limb wearable robotics, such as exoskeletons, while walking. The sensor characteristics were evaluated using a testing machine and walking experiments on an instrumented treadmill. Using the results from the testing machine, the sensor proved suitable for use in an insole application for controlling wearable robotics during human walking with respect to sensitivity, minimal detectable change, hysteresis, drift, and repeatability. The evaluation of these sensor characteristics establishes a benchmark for ferroelectret-based sensors regarding methodology and identified sensor properties. However, we found that the sensitivity of the sensor output is affected by the interfacing material. In the case of the insole application, this material is the wearer's foot sole, which has different properties from one person to another. Based on our proof-of-concept experiment, the impact of this variability on gait event detection needs to be further investigated in future studies, incorporating multiple participants.

Walking experiments revealed that heel strike and toe-off detection is possible with minimal deviation and variability compared to our reference based on vertical ground reaction

forces. The deviations are below the level of significant impact on the functionality of lower limb wearable robots such as exoskeletons. In addition, the detection can be faster than force measurement plates and other commercial insoles, which offers enhanced disturbance compensation and additional buffer time in real-time control. With our evaluation, we lay the foundations for the extraction of additional biomechanical characteristics based on the insole data, while the customizability through 3D printing allows for an increase of spatial resolution and potential extension towards multi-axial measurements. Estimating features, such as the walking speed, spatio-temporal characteristics, the pressure distribution, and the center of pressure, not only facilitates their utilization in robotic control but also enhances the functionality of the insole as an autonomous biomechanical measurement device, with minimal impact on the natural gait.

#### REFERENCES

- [1] V. Dietz and J. Duysens, "Significance of load receptor input during locomotion: A review," *Gait & Posture*, vol. 11, no. 2, pp. 102–110, 2000. DOI: [10.1016/s0966-6362\(99\)00052-1](https://doi.org/10.1016/s0966-6362(99)00052-1).
- [2] D. Kotiadis *et al.*, "Inertial Gait Phase Detection for control of a drop foot stimulator," *Med. Eng. Phys.*, vol. 32, no. 4, pp. 287–297, 2010. DOI: [10.1016/j.medengphy.2009.10.014](https://doi.org/10.1016/j.medengphy.2009.10.014).
- [3] I. Kang *et al.*, "Real-Time Neural Network-Based Gait Phase Estimation Using a Robotic Hip Exoskeleton," *IEEE Trans. Med. Robot. Bionics*, vol. 2, no. 1, pp. 28–37, 2020. DOI: [10.1109/tmrb.2019.2961749](https://doi.org/10.1109/tmrb.2019.2961749).
- [4] J. Lee *et al.*, "Continuous Gait Phase Estimation Using LSTM for Robotic Transfemoral Prosthesis Across Walking Speeds," *IEEE Trans. Neural Syst. Rehabil. Eng.*, vol. 29, pp. 1470–1477, 2021. DOI: [10.1109/tnsre.2021.3098689](https://doi.org/10.1109/tnsre.2021.3098689).
- [5] P. M. Kennedy and J. T. Inglis, "Distribution and behaviour of glabrous cutaneous receptors in the human foot sole," *J. Physiol.*, vol. 538, no. 3, pp. 995–1002, 2002. DOI: [10.1113/jphysiol.2001.013087](https://doi.org/10.1113/jphysiol.2001.013087).
- [6] K. G. Pearson, "Proprioceptive regulation of locomotion," *Curr. Opin. Neurobiol.*, vol. 5, no. 6, pp. 786–791, 1995. DOI: [10.1016/0959-4388\(95\)80107-3](https://doi.org/10.1016/0959-4388(95)80107-3).
- [7] M. Grimmer *et al.*, "Human Lower Limb Joint Biomechanics in Daily Life Activities: A Literature Based Requirement Analysis for Anthropomorphic Robot Design," *Front. Robot. AI*, vol. 7, Art. no. 13, 2020. DOI: [10.3389/frobt.2020.00013](https://doi.org/10.3389/frobt.2020.00013).
- [8] D.-H. Lim *et al.*, "Development of real-time gait phase detection system for a lower extremity exoskeleton robot," *Int. J. Precis. Eng. Manuf.*, vol. 18, no. 5, pp. 681–687, 2017. DOI: [10.1007/s12541-017-0081-9](https://doi.org/10.1007/s12541-017-0081-9).
- [9] O. N. Beck *et al.*, "Exoskeletons need to react faster than physiological responses to improve standing balance," *Sci. Robot.*, vol. 8, no. 75, eadf1080, 2023. DOI: [10.1126/scirobotics.adf1080](https://doi.org/10.1126/scirobotics.adf1080).
- [10] C. Hubicki *et al.*, "Walking and Running with Passive Compliance: Lessons from Engineering: A Live Demonstration of the ATRIAS Biped," *IEEE Robot. Automat. Mag.*, vol. 25, no. 3, pp. 23–39, 2018. DOI: [10.1109/mra.2017.2783922](https://doi.org/10.1109/mra.2017.2783922).
- [11] S. Viteckova *et al.*, "Gait symmetry measures: A review of current and prospective methods," *Biomed. Signal Process. Control.*, vol. 42, pp. 89–100, 2018. DOI: [10.1016/j.bspc.2018.01.013](https://doi.org/10.1016/j.bspc.2018.01.013).
- [12] A. Ancillao *et al.*, "Indirect Measurement of Ground Reaction Forces and Moments by Means of Wearable Inertial Sensors: A Systematic Review," *Sensors*, vol. 18, no. 8, Art. no. 2564, 2018. DOI: [10.3390/s18082564](https://doi.org/10.3390/s18082564).
- [13] O. Mohseni *et al.*, "Unified GRF-based control for adjusting hopping frequency with various robot configurations," *Adv. Robot.*, vol. 36, no. 13, pp. 641–653, 2022. DOI: [10.1080/01691864.2022.2077637](https://doi.org/10.1080/01691864.2022.2077637).
- [14] O. Mohseni *et al.*, "Bioinspired Legged Robot Design via Blended Physical and Virtual Impedance Control," *J. Intell. Robot. Syst.*, vol. 105, no. 1, Art. no. 22, 2022. DOI: [10.1007/s10846-022-01631-2](https://doi.org/10.1007/s10846-022-01631-2).
- [15] J. Perry and J. M. Burnfield, Eds., *Gait Analysis: Normal and Pathological Function*, 2nd ed. Thorofare, NJ, USA: SLACK, 2010, 576 pp.

- [16] D. A. Neumann *et al.*, *Kinesiology of the Musculoskeletal System: Foundations for Rehabilitation*, Third edition. St. Louis, Missouri: Elsevier, 2017, 766 pp.
- [17] J. Leitch *et al.*, "Identifying gait events without a force plate during running: A comparison of methods," *Gait & Posture*, vol. 33, no. 1, pp. 130–132, 2011. DOI: [10.1016/j.gaitpost.2010.06.009](https://doi.org/10.1016/j.gaitpost.2010.06.009).
- [18] V. Tsakanikas *et al.*, "Evaluating Gait Impairment in Parkinsons Disease from Instrumented Insole and IMU Sensor Data," *Sensors*, vol. 23, no. 8, Art. no. 3902, 2023. DOI: [10.3390/s23083902](https://doi.org/10.3390/s23083902).
- [19] F. A. Garcia *et al.*, "Adaptive Algorithm for Gait Segmentation Using a Single IMU in the Thigh Pocket," *IEEE Sens. J.*, vol. 22, no. 13, pp. 13 251–13 261, 2022. DOI: [10.1109/jсен.2022.3177951](https://doi.org/10.1109/jсен.2022.3177951).
- [20] L. Wang *et al.*, "A Portable Insole System to Simultaneously Measure Plantar Pressure and Shear Stress," *IEEE Sens. J.*, vol. 22, no. 9, pp. 9104–9113, 2022. DOI: [10.1109/jсен.2022.3162713](https://doi.org/10.1109/jсен.2022.3162713).
- [21] P. Catalfamo *et al.*, "Detection of gait events using an F-Scan in-shoe pressure measurement system," *Gait & Posture*, vol. 28, no. 3, pp. 420–426, 2008. DOI: [10.1016/j.gaitpost.2008.01.019](https://doi.org/10.1016/j.gaitpost.2008.01.019).
- [22] A. Putti *et al.*, "The Pedar in-shoe system: Repeatability and normal pressure values," *Gait & Posture*, vol. 25, no. 3, pp. 401–405, 2007. DOI: [10.1016/j.gaitpost.2006.05.010](https://doi.org/10.1016/j.gaitpost.2006.05.010).
- [23] W. Seiberl *et al.*, "Accuracy and precision of loadsol insole force-sensors for the quantification of ground reaction force-based biomechanical running parameters," *Eur. J. Sport Sci.*, vol. 18, no. 8, pp. 1100–1109, 2018. DOI: [10.1080/17461391.2018.1477993](https://doi.org/10.1080/17461391.2018.1477993).
- [24] B. J. Braun *et al.*, "Validation and reliability testing of a new, fully integrated gait analysis insole," *J. Foot Ankle Res.*, vol. 8, no. 1, Art. no. 54, 2015. DOI: [10.1186/s13047-015-0111-8](https://doi.org/10.1186/s13047-015-0111-8).
- [25] B. Eskofier *et al.*, "An Overview of Smart Shoes in the Internet of Health Things: Gait and Mobility Assessment in Health Promotion and Disease Monitoring," *Appl. Sci.*, vol. 7, no. 10, Art. no. 986, 2017. DOI: [10.3390/app7100986](https://doi.org/10.3390/app7100986).
- [26] I. Almuteb *et al.*, "Smart insoles review (2008-2021): Applications, potentials, and future," *Smart Health*, vol. 25, Art. no. 100301, 2022. DOI: [10.1016/j.smhl.2022.100301](https://doi.org/10.1016/j.smhl.2022.100301).
- [27] S. Negi *et al.*, "FSR and IMU sensors-based human gait phase detection and its correlation with EMG signal for different terrain walk," *Sens. Rev.*, vol. 41, no. 3, pp. 235–245, 2021. DOI: [10.1108/sr-10-2020-0249](https://doi.org/10.1108/sr-10-2020-0249).
- [28] S. Subramaniam *et al.*, "Insole-Based Systems for Health Monitoring: Current Solutions and Research Challenges," *Sensors*, vol. 22, no. 2, Art. no. 438, 2022. DOI: [10.3390/s22020438](https://doi.org/10.3390/s22020438).
- [29] H. Abou Ghaida *et al.*, "Effect of Sensor Size, Number and Position under the Foot to Measure the Center of Pressure (CoP) Displacement and Total Center of Pressure (CoPT) Using an Anatomical Foot Model," *Sensors*, vol. 23, no. 10, Art. no. 4848, 2023. DOI: [10.3390/s23104848](https://doi.org/10.3390/s23104848).
- [30] P. R. Cavanagh *et al.*, "In-shoe plantar pressure measurement: A review," *The Foot*, vol. 2, no. 4, pp. 185–194, 1992. DOI: [10.1016/0958-2592\(92\)90047-s](https://doi.org/10.1016/0958-2592(92)90047-s).
- [31] J. A. Ramirez-Bautista *et al.*, "A Review in Detection and Monitoring Gait Disorders Using In-Shoe Plantar Measurement Systems," *IEEE Rev. Biomed. Eng.*, vol. 10, pp. 299–309, 2017. DOI: [10.1109/rbme.2017.2747402](https://doi.org/10.1109/rbme.2017.2747402).
- [32] B. Smith *et al.*, "Evaluation of force-sensing resistors for gait event detection to trigger electrical stimulation to improve walking in the child with cerebral palsy," *IEEE Trans. Neural Syst. Rehabil. Eng.*, vol. 10, no. 1, pp. 22–29, 2002. DOI: [10.1109/tnsre.2002.1021583](https://doi.org/10.1109/tnsre.2002.1021583).
- [33] S. Bamberg *et al.*, "Gait Analysis Using a Shoe-Integrated Wireless Sensor System," *IEEE Trans. Inform. Technol. Biomed.*, vol. 12, no. 4, pp. 413–423, 2008. DOI: [10.1109/titb.2007.899493](https://doi.org/10.1109/titb.2007.899493).
- [34] L. Shu *et al.*, "In-Shoe Plantar Pressure Measurement and Analysis System Based on Fabric Pressure Sensing Array," *IEEE Trans. Inform. Technol. Biomed.*, vol. 14, no. 3, pp. 767–775, 2010. DOI: [10.1109/titb.2009.2038904](https://doi.org/10.1109/titb.2009.2038904).
- [35] F. Lin *et al.*, "Smart Insole: A Wearable Sensor Device for Unobtrusive Gait Monitoring in Daily Life," *IEEE Trans. Ind. Inf.*, vol. 12, no. 6, pp. 2281–2291, 2016. DOI: [10.1109/tii.2016.2585643](https://doi.org/10.1109/tii.2016.2585643).
- [36] B. Nie *et al.*, "TextileBased Wireless Pressure Sensor Array for HumanInteractive Sensing," *Adv. Funct. Mater.*, vol. 29, no. 22, Art. no. 1 808 786, 2019. DOI: [10.1002/adfm.201808786](https://doi.org/10.1002/adfm.201808786).
- [37] C. Deng *et al.*, "Self Powered Insole Plantar Pressure Mapping System," *Adv. Funct. Mater.*, vol. 28, no. 29, Art. no. 1 801 606, 2018. DOI: [10.1002/adfm.201801606](https://doi.org/10.1002/adfm.201801606).
- [38] M. Zhu *et al.*, "Self-Powered and Self-Functional Cotton Sock Using Piezoelectric and Triboelectric Hybrid Mechanism for Healthcare and Sports Monitoring," *ACS Nano*, vol. 13, no. 2, pp. 1940–1952, 2019. DOI: [10.1021/acsnano.8b08329](https://doi.org/10.1021/acsnano.8b08329).
- [39] S. Gao *et al.*, "Piezoelectric-Based Insole Force Sensing for Gait Analysis in the Internet of Health Things," *IEEE Consumer Electron. Mag.*, vol. 10, no. 1, pp. 39–44, 2021. DOI: [10.1109/mce.2020.2986828](https://doi.org/10.1109/mce.2020.2986828).
- [40] S. Rajala *et al.*, "Designing, Manufacturing and Testing of a Piezoelectric Polymer Film In-Sole Sensor for Plantar Pressure Distribution Measurements," *IEEE Sens. J.*, vol. 17, no. 20, pp. 6798–6805, 2017. DOI: [10.1109/jсен.2017.2750241](https://doi.org/10.1109/jсен.2017.2750241).
- [41] D. Vilarinho *et al.*, "POFBG-Embedded Cork Insole for Plantar Pressure Monitoring," *Sensors*, vol. 17, no. 12, Art. no. 2924, 2017. DOI: [10.3390/s17122924](https://doi.org/10.3390/s17122924).
- [42] Z. Hao *et al.*, "3-D Printed Smart Orthotic Insoles: Monitoring a Person's Gait Step by Step," *IEEE Sens. Lett.*, vol. 4, no. 1, pp. 1–4, 2020. DOI: [10.1109/lsens.2019.2962270](https://doi.org/10.1109/lsens.2019.2962270).
- [43] Z. Lin *et al.*, "A Triboelectric NanogeneratorBased Smart Insole for Multifunctional Gait Monitoring," *Adv. Mater. Technol.*, vol. 4, no. 2, Art. no. 1 800 360, 2019. DOI: [10.1002/admt.201800360](https://doi.org/10.1002/admt.201800360).
- [44] M. Saito *et al.*, "An in-shoe device to measure plantar pressure during daily human activity," *Med. Eng. Phys.*, vol. 33, no. 5, pp. 638–645, 2011. DOI: [10.1016/j.medengphy.2011.01.001](https://doi.org/10.1016/j.medengphy.2011.01.001).
- [45] I. Acharya *et al.*, "A Force-Sensing Insole to Quantify Impact Loading to the Foot," *J. Biomech. Eng.*, vol. 141, no. 2, Art. no. 024 501, 2019. DOI: [10.1115/1.4041902](https://doi.org/10.1115/1.4041902).
- [46] J. Low *et al.*, "A pressure-redistributing insole using soft sensors and actuators," in *2015 IEEE International Conference on Robotics and Automation (ICRA)*, Seattle, WA, USA: IEEE, 2015, pp. 2926–2930. DOI: [10.1109/icra.2015.7139599](https://doi.org/10.1109/icra.2015.7139599).
- [47] E. I. G. Velásquez *et al.*, "Error compensation in force sensing resistors," *Sens. Bio-Sens. Res.*, vol. 26, Art. no. 100300, 2019. DOI: [10.1016/j.sbsr.2019.100300](https://doi.org/10.1016/j.sbsr.2019.100300).
- [48] B. Latsch *et al.*, "Low Creep 3D-Printed Piezoresistive Force Sensor for Structural Integration," in *2023 IEEE Sensors*, Vienna, Austria: IEEE, 2023, pp. 1–4. DOI: [10.1109/sensors56945.2023.10325114](https://doi.org/10.1109/sensors56945.2023.10325114).
- [49] L. Paredes-Madrid *et al.*, "Underlying Physics of Conductive Polymer Composites and Force Sensing Resistors (FSRs). A Study on Creep Response and Dynamic Loading," *Materials*, vol. 10, no. 11, Art. no. 1334, 2017. DOI: [10.3390/ma10111334](https://doi.org/10.3390/ma10111334).
- [50] H. Prasanth *et al.*, "Wearable Sensor-Based Real-Time Gait Detection: A Systematic Review," *Sensors*, vol. 21, no. 8, Art. no. 2727, 2021. DOI: [10.3390/s21082727](https://doi.org/10.3390/s21082727).
- [51] C. Price *et al.*, "Validity and repeatability of three in-shoe pressure measurement systems," *Gait & Posture*, vol. 46, pp. 69–74, 2016. DOI: [10.1016/j.gaitpost.2016.01.026](https://doi.org/10.1016/j.gaitpost.2016.01.026).
- [52] S. Bauer *et al.*, "Ferroelectrets: Soft Electroactive Foams for Transducers," *Physics Today*, vol. 57, no. 2, pp. 37–43, 2004. DOI: [10.1063/1.1688068](https://doi.org/10.1063/1.1688068).
- [53] Y. A. O. Assagra *et al.*, "A new route to piezo-polymer transducers: 3D printing of polypropylene ferroelectrets," *IEEE Trans. Dielect. Electr. Insul.*, vol. 27, no. 5, pp. 1668–1674, 2020. DOI: [10.1109/tdei.2020.008461](https://doi.org/10.1109/tdei.2020.008461).
- [54] O. Ben Dali *et al.*, "Eco-Friendly High-Sensitive Piezoelectrets for Force Myography," *IEEE Sens. J.*, vol. 23, no. 3, pp. 1943–1951, 2023. DOI: [10.1109/jсен.2022.3225723](https://doi.org/10.1109/jсен.2022.3225723).
- [55] H. von Seggern *et al.*, "Highly Efficient Piezoelectrets through Ultra-Soft Elastomeric Spacers," *Polymers*, vol. 13, no. 21, Art. no. 3751, 2021. DOI: [10.3390/polym13213751](https://doi.org/10.3390/polym13213751).
- [56] O. Ben Dali *et al.*, "Ferroelectret energy harvesting with 3Dprinted airspaced cantilever design," *Nano Select*, vol. 3, no. 3, pp. 713–722, 2022. DOI: [10.1002/nano.202100210](https://doi.org/10.1002/nano.202100210).
- [57] O. Ben Dali *et al.*, "Cantilever-based ferroelectret energy harvesting," *Appl. Phys. Lett.*, vol. 116, no. 24, Art. no. 243 901, 2020. DOI: [10.1063/5.0006620](https://doi.org/10.1063/5.0006620).
- [58] M. L. Di Lorenzo and R. Androsch, Eds., *Industrial Applications of Poly(Lactic Acid)* (Advances in Polymer Science 282). Cham: Springer International Publishing, 2018, 228 pp. DOI: [10.1007/978-3-319-75459-8](https://doi.org/10.1007/978-3-319-75459-8).
- [59] S. Zhukov *et al.*, "Biodegradable cellular polylactic acid ferroelectrets with strong longitudinal and transverse piezoelectricity," *Appl. Phys. Lett.*, vol. 117, no. 11, Art. no. 112 901, 2020. DOI: [10.1063/5.0023153](https://doi.org/10.1063/5.0023153).
- [60] H. Kaczmarek *et al.*, "Advances in the study of piezoelectric polymers," *Russ. Chem. Rev.*, vol. 88, no. 7, pp. 749–774, 2019. DOI: [10.1070/rcr4860](https://doi.org/10.1070/rcr4860).

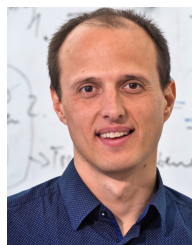
- [61] E. J. Curry *et al.*, "Biodegradable Piezoelectric Force Sensor," *Proc. Natl. Acad. Sci. U.S.A.*, vol. 115, no. 5, pp. 909–914, 2018. DOI: [10.1073/pnas.1710874115](https://doi.org/10.1073/pnas.1710874115).
- [62] X. Ma *et al.*, "Disposable sensors based on biodegradable polylactic acid piezoelectret films and their application in wearable electronics," *Sens. Actuator A Phys.*, vol. 346, Art. no. 113 834, 2022. DOI: [10.1016/j.sna.2022.113834](https://doi.org/10.1016/j.sna.2022.113834).
- [63] O. Ben Dali *et al.*, "Ultrasensitive and low-cost insole for gait analysis using piezoelectrets," in *2022 IEEE Sensors*, Dallas, TX, USA: IEEE, 2022, pp. 1–4. DOI: [10.1109/sensors52175.2022.9967198](https://doi.org/10.1109/sensors52175.2022.9967198).
- [64] Y. Sellami *et al.*, "Piezoelectret Sensors from Direct 3D-Printing onto Bulk Films," in *2023 IEEE Sensors*, Vienna, Austria: IEEE, 2023, pp. 1–4. DOI: [10.1109/sensors56945.2023.10324862](https://doi.org/10.1109/sensors56945.2023.10324862).
- [65] L. Donath *et al.*, "Validity and reliability of a portable gait analysis system for measuring spatiotemporal gait characteristics: Comparison to an instrumented treadmill," *J. NeuroEng. Rehabil.*, vol. 13, Art. no. 6, 2016. DOI: [10.1186/s12984-016-0115-z](https://doi.org/10.1186/s12984-016-0115-z).
- [66] L.-N. Veilleux *et al.*, "Agreement of spatio-temporal gait parameters between a vertical ground reaction force decomposition algorithm and a motion capture system," *Gait & Posture*, vol. 43, pp. 257–264, 2016. DOI: [10.1016/j.gaitpost.2015.10.007](https://doi.org/10.1016/j.gaitpost.2015.10.007).
- [67] H. Kinoshita *et al.*, "The mechanical properties of the heel pad in elderly adults," *Europ. J. Appl. Physiol.*, vol. 73, no. 5, pp. 404–409, 1996. DOI: [10.1007/bf00334416](https://doi.org/10.1007/bf00334416).
- [68] Y. P. Raizer, *Gas Discharge Physics*, J. E. Allen, Ed. Berlin: Springer, 1991, 449 pp.
- [69] J. Hillenbrand and G. Sessler, "Piezoelectricity in cellular electret films," *IEEE Trans. Dielect. Electr. Insul.*, vol. 7, no. 4, pp. 537–542, 2000. DOI: [10.1109/94.868074](https://doi.org/10.1109/94.868074).
- [70] P. Regtien and E. Dertien, "Piezoelectric sensors," in *Sensors for Mechatronics*, Elsevier, 2018, pp. 245–265. DOI: [10.1016/b978-0-12-813810-6.00008-2](https://doi.org/10.1016/b978-0-12-813810-6.00008-2).
- [71] H.-J. Lee *et al.*, "A Wearable Hip Assist Robot Can Improve Gait Function and Cardiopulmonary Metabolic Efficiency in Elderly Adults," *IEEE Trans. Neural Syst. Rehabil. Eng.*, pp. 1549–1557, 2017. DOI: [10.1109/tnsrse.2017.2664801](https://doi.org/10.1109/tnsrse.2017.2664801).
- [72] G. Papanicolaou and S. Zaoutos, "Viscoelastic constitutive modeling of creep and stress relaxation in polymers and polymer matrix composites," in *Creep and Fatigue in Polymer Matrix Composites*, Elsevier, 2019, pp. 3–59. DOI: [10.1016/b978-0-08-102601-4.00001-1](https://doi.org/10.1016/b978-0-08-102601-4.00001-1).
- [73] C. Tudor-Locke and D. R. Bassett, "How Many Steps/Day Are Enough?: Preliminary Pedometer Indices for Public Health," *Sports Med.*, vol. 34, no. 1, pp. 1–8, 2004. DOI: [10.2165/00007256-200434010-00001](https://doi.org/10.2165/00007256-200434010-00001).
- [74] B. Latsch *et al.*, *Dataset for Event Detection in Gait Analysis from 3D-Printed Piezoelectric PLA-Based Insole on an Instrumented Treadmill*, Technische Universität Darmstadt, 2024. DOI: [10.48328/tudatalib-1360](https://doi.org/10.48328/tudatalib-1360).
- [75] J. M. Burnfield *et al.*, "The influence of walking speed and footwear on plantar pressures in older adults," *Clin. Biomech.*, vol. 19, no. 1, pp. 78–84, 2004. DOI: [10.1016/j.clinbiomech.2003.09.007](https://doi.org/10.1016/j.clinbiomech.2003.09.007).
- [76] J. Lee *et al.*, "Effects of assistance timing on metabolic cost, assistance power, and gait parameters for a hip-type exoskeleton," in *2017 International Conference on Rehabilitation Robotics (ICORR)*, London, UK: IEEE, 2017, pp. 498–504. DOI: [10.1109/icorr.2017.8009297](https://doi.org/10.1109/icorr.2017.8009297).
- [77] J. M. Jasiewicz *et al.*, "Gait event detection using linear accelerometers or angular velocity transducers in able-bodied and spinal-cord injured individuals," *Gait & Posture*, vol. 24, no. 4, pp. 502–509, 2006. DOI: [10.1016/j.gaitpost.2005.12.017](https://doi.org/10.1016/j.gaitpost.2005.12.017).
- [78] J. Kim *et al.*, "Gait event detection algorithm based on smart insoles," *ETRI J.*, vol. 42, no. 1, pp. 46–53, 2020. DOI: [10.4218/etrij.2018-0639](https://doi.org/10.4218/etrij.2018-0639).



**Bastian Latsch** received the M.Sc. degree in electrical engineering from Technische Universität Darmstadt, Darmstadt, Germany, in 2019, where he is currently pursuing the Ph.D. degree in electrical engineering with the Measurement and Sensor Technology Group. His research interests include sensors in human movement assistance and interfaces for human-machine interaction.



**Niklas Schäfer** received the M.Sc. degree in electrical engineering from Technische Universität Darmstadt, Darmstadt, Germany, in 2018. He is currently pursuing the Ph.D. degree in electrical engineering at the Measurement and Sensor Technology Group, Technische Universität Darmstadt. His research interests include wearable robotics and interfaces for human-machine interaction, with a focus on wearable sensors and haptics.



**Martin Grimmer** received a diploma in sports science at FSU Jena (2008) and a PhD (2015) at TU Darmstadt, Germany. He was a guest researcher at the Arizona State University (2012) and Postdoc at Harvard (2015) and at the ETH Zurich (2016/17). Currently he is an Athene Young Investigator group leader at TU Darmstadt. His research interests include biomechanics of human movement, the transfer of biological inspired mechanical principles to wearable robotics, human-robot interaction, and wearable

robotics control.



**Omar Ben Dali** received the M.Sc. degree in 2018 and the Ph.D. degree in 2023 in electrical engineering from the Technische Universität Darmstadt, Darmstadt, Germany. Since then, he has been a postdoctoral researcher with the Measurement and Sensor Technology Group, Technische Universität Darmstadt. His research interests include the design of flexible transducers and energy harvesters.



**Omid Mohseni** received the M.Sc. in Electrical Engineering with a specialization in Control Engineering from the University of Tehran in 2017. He has been a research associate at the Cognitive Systems Laboratory, University of Tehran, and at Laufflabor Locomotion Laboratory, TU Darmstadt. Currently, he is pursuing a Ph.D. in the Department of Electrical Engineering and Information Technology at TU Darmstadt under the co-supervision of Prof. Andre Seyfarth and Prof. Mario Kupnik. His research interests focus

on the biomechanics of human locomotion, bioinspired legged robotics, and wearable robotics control.



**Niklas Bleichner** received a M.Sc. degree in sport science with a specialization in biomechanics from Karlsruhe Institute of Technology, Germany, in 2022. Presently, he is enrolled in a Ph.D. program (LokoAssist) within the MotionLab of Prof. Sebastian Wolf located in the Department of Orthopedics at Heidelberg University Hospital. He is passionate about medical decision making in clinical practice based on biomechanical analysis, Niklas's research focuses on orthotic and prosthetic treatment methods for individuals with gait disorders. His current research is about how functional electrical stimulation can influence not just the biomechanics but also the well-being and dual-task ability of individuals with neuromuscular impairments.



**André Seyfarth** received the Vordiplom degree in physics in 1991, the Diploma degree (including B.Sc. and M.Sc.) in physics and biomechanics in 1995, and the Ph.D. degree in biomechanics in 2000 all from Friedrich-Schiller-Universität Jena, Germany. He is a Professor for Sports Biomechanics with the Department of Human Sciences of Technische Universität Darmstadt, Germany, and the Head of the Laufflabor Locomotion Laboratory. After his studies, he was a DFG Emmy Noether Fellow with the MIT LegLab (Prof. Herr, USA) and the ParaLab, University Hospital Balgrist, Zurich (Prof. Dietz, Switzerland). His research interests include sport science, human and animal biomechanics, and legged robots. Prof. Seyfarth was the organizer of the Dynamic Walking 2011 conference (Principles and Concepts of Legged Locomotion) and the AMAM 2013 conference (Adaptive Motions in Animals and Machines).



**Alexander A. Altmann** received the M.Sc. degree in information systems technology from the Technische Universität Darmstadt, Germany, in 2021. Since 2022, he has been a Research Associate with the Measurement and Sensor Technology Group, Technische Universität Darmstadt. His research interests include the additive manufacturing of flexible sensors based on ferroelectrets and the integration into human-centric applications, such as textile integration or medical applications.



**Philipp Beckerle** (Senior Member, IEEE) received his Dr.-Ing. in mechatronics from Technische Universität Darmstadt, Germany, in 2014 and his habilitation from Technische Universität Dortmund, Germany, in 2021. He is full professor and chair of Autonomous Systems and Mechatronics at Friedrich-Alexander-Universität Erlangen-Nürnberg, Germany, and was visiting researcher at Vrije Universiteit Brussel, Arizona State University, and University of Siena. He takes over review and editorial responsibilities for various international journals and conferences. His main research topics are human-centered design, elastic actuation, wearable robotics, and human-robot interaction. Prof. Beckerle's dissertation was awarded the Manfred-Hirschvogel Award 2015 and the MINT Excellence Ph.D. thesis award 2015. He was the recipient of the Eugen-Hartmann Award 2017 and the Athene Young Investigator grant in 2017.



**Stephan Schaumann** received the M.Sc. degree in mechatronics from Technische Universität Darmstadt, Germany, in 2022. He is currently pursuing the Ph.D. degree in electrical engineering at the Measurement and Sensor Technology Group, Technische Universität Darmstadt. His research interests include sensors in human movement assistance, ferroelectret-based transducers, and ultrasonic transducers.



**Mario Kupnik** (Senior Member, IEEE) received the Diplom-Ingenieur degree in electrical engineering from Graz University of Technology, Graz, Austria, in 2000, and the Ph.D. degree in electrical engineering from the University of Leoben, Leoben, Austria, in 2004. From 2005 to 2011, he was working as a Postdoctoral Researcher, a Research Associate, and a Senior Research Scientist at the Edward L. Ginzton Laboratory, Stanford University, Stanford, CA, USA. From 2011 to 2014, he was a Full Professor of electrical engineering at the Brandenburg University of Technology, Cottbus, Germany. Since 2015, he has been a Full Professor at Technische Universität Darmstadt, Germany, where he is currently the Head of the Measurement and Sensor Technology Group. His research topics are micromachined sensors and actuators, multiphysics simulations, ferroelectrets, flowmetering of gases and liquids, ultrasound, electroacoustics, human-machine interaction and robotics.



**Sebastian I. Wolf** received a PhD degree in physics at Free University in Berlin, Germany, in 1998 and spent several years in fundamental research in physics at Max-Planck-Institute for Nuclear Science in Heidelberg. He changed to the field of Human Movement Analysis in 2001 and became Technical Director of the Gait Analysis Laboratory in the Department of Orthopaedic Surgery at Heidelberg University. In 2018 he was awarded as extra-ordinary professor for Orthopedic Biomechanics at the Medical Faculty of Heidelberg University. He founded the German speaking society for gait analysis GAMMA in 2005 which he lead until 2013. He was also president of the European Society for Movement Analysis in Adults and Children (ESMAC) in the years 2015 to 2019. Sebastian Wolf is active in clinical motion analysis with continuing scientific interest in advancing knowledge on neurologic and orthopedic gait disorders and mobility related medical healthcare, specifically in prosthetics and orthotics.